Direct links between hygroscopicity and mixing state of ambient aerosols: Estimating particle hygroscopicity from their single particle mass spectra

Xinning Wang[1], Xingnan Ye[1], Jianmin Chen[1], Xiaofei Wang*[1,2], Xin Yang*[1,2,3],

Tzung-May Fu[3], Lei Zhu[3], Chongxuan Liu[3]

[1] Shanghai Key Laboratory of Atmospheric Particle Pollution and Prevention, Department of Environmental Science and Engineering, Fudan University, Shanghai, China

[2] Shanghai Institute of Pollution Control and Ecological Security, Shanghai, China

[3] School of Environmental Science and Engineering, Southern University of Science and Technology, Shenzhen, China

Atmospheric Chemistry and Physics

April 2nd, 2020

*To whom correspondence should be addressed.

Correspondence to:

Xiaofei Wang: Email: xiaofeiwang@fudan.edu.cn Tel: +86-21-31242526

Xin Yang: Email: yangxin@fudan.edu.cn Tel: +86-21-31245272

ABSTRACT

Hygroscopicity plays crucial roles in determining aerosol optical properties and aging processes in the atmosphere. We investigated submicron aerosol hygroscopicity and composition by connecting an aerosol time-of-flight mass spectrometer (ATOFMS) in series to a hygroscopic tandem differential mobility analyzer (HTDMA), to characterize hygroscopicity and composition of ambient aerosols in Shanghai, China. The HTDMA-ATOFMS data suggested that particle types, including biomass burning, EC, Dust/Ash, organics particles, cooking particles and sea salt, were shown to have distinct hygroscopicity distributions. Peak intensities in particle spectra were found nonlinearly correlated with hygroscopicity and the correlations were variant with particle types. Based on the measured hygroscopicity-composition relations, we developed a statistical method to estimate ambient particle hygroscopicity just from their mass spectra. The method was applied to another ambient ATOFMS dataset sampled during September 12nd to 28th, 2012 in Shanghai. The estimated hygroscopicity suggested that ambient particles were present in three apparent hygroscopicity modes, whose growth factors peaked at 1.05, 1.42 and 1.60 (85% RH), respectively. The estimated GF were divided into four bins as <1.1, 1.1-1.3, 1.3-1.5 and >1.5 to represent the nearly-hydrophobic (NH), less-hygroscopic (LH), more-hygroscopic (MH) and sea salt (SS) mode. Number contributions of particle types to hygroscopicity modes showed consistent results with the HTDAM-ATOFMS experiment. Based on the combined information on particle composition, hygroscopicity, airmass back trajectories and ambient pollutants concentrations, we inferred that the NH, LH, MH, SS modes were characterized by POA/EC, SOA, SIA and salts compositions, respectively. The proposed method would provide additional information to the study of particle mixing states, source identification and visibility degradation.

1. INTRODUCTION

Atmospheric particles have critical impacts on climate and the environment. They affect climate by directly interacting with sunlight and changing the energy balance of earth's atmosphere (Facchini et al., 1999;Lohmann and Feichter, 2005). Aerosol particles also act as cloud condensation nuclei or ice nuclei and impact cloud formation (Lohmann and Feichter, 2005). Aerosol particles provide surfaces for heterogeneous reactions to occur and act as the sink for many atmospheric reactions (Gard et al., 1998;Qiu and Zhang, 2013), which are of significance to air quality, visibility and human health. The climate-relevant and other properties of aerosols are largely determined by their hygroscopicity. In atmospheric conditions the hygroscopic growth transform particles into micro droplets and their optical effects are altered importantly (Cheng et al., 2008;Qu et al., 2015), which further impacts particle aging processes and visibility degradation (Qu et al., 2015;Liu et al., 2012;Qiu and Zhang, 2013;Chen et al., 2012).

Atmospheric particles are a mixture of a complicated variety of chemical compounds. The bulk chemical composition of particulate matter (PM) usually refers to its dry composition. However, in ambient conditions the particulate water is also an important constitution of PM which has not been accounted for in conventional gravitational analysis. The mass of particulate water may be much larger than the total mass of dried PM at elevated RHs (Swietlicki et al., 2008). The factors that affect water contents in particles include the particle hygroscopicity, the particle size distributions and ambient RH. The hygroscopicity parameter determines the particle's ability to growth in their sizes in humidity environment, which is directly relates to particle composition and size. To accurately predict particulate water content, a detailed knowledge on particle hygroscopicity and composition is needed (Gysel et al., 2007;Sjogren et al., 2008;Laborde et al., 2013;Healy et al., 2014).

Aerosol hygroscopicity can be quantitatively measured by techniques such as the Hygroscopic Tandem Differential Mobility Analyzer (HTDMA) (Swietlicki et al., 2008). Previous studies measured aerosol hygroscopicity and chemical composition simultaneously by deploying HTDMA and chemical composition measurements in parallel (Gysel et al., 2007;Sjogren et al., 2008;Laborde et al., 2013). The measured hygroscopicity was compared with the reconstructed values using the mixing rules of variant compositions (Gysel et al., 2007). The hygroscopicity

77 reconstructed in this way is representing the averaged hygroscopicity of ensembled particles

78 and therefore could not reflect the mixing states of particles (Healy et al., 2014). However, the

79 HTDMA measurements suggested that several hygroscopicity modes exist simultaneously,

80 which evidenced the external mixing state of atmospheric particles. HTDMA hygroscopicity

81 modes were generally fell into four categories: nearly hydrophobic (NH), less-hygroscopic

82 (LH), more-hygroscopic (MH), and sea-salt mode, with their center GFs (90% RH) lie in 1.0-

83 1.11, 1.11-1.33, >1.33 and >1.8 ranges, respectively (Swietlicki et al., 2008). To investigate the

84 chemical nature of these hygroscopicity modes, it is better to connect HTDMA and composition

85 measurement techniques in tandem, since more direct connection between hygroscopicity and

86 composition could be established in this way (Buzorius et al., 2002;Zelenyuk et al.,

87 2008;Herich et al., 2008;Laborde et al., 2013). For composition measurement techniques, single

88 particle mass spectrometers are preferred since they are sensitive to analyze particles of low

89 concentrations in the HTDMA outflow (Herich et al., 2008;Herich et al., 2009), and that the

90 particle mixing state information is preserved during analysis (Healy et al., 2014).

91 Only a few studies have reported simultaneous characterization of hygroscopicity and

92 composition using the tandem method (Herich et al., 2008;Herich et al., 2009;Buzorius et al.,

93 2002;Zelenyuk et al., 2008). Zelenyuk et al. connected a single particle mass spectrometer

94 SPLAT with HTDMA to demonstrate the capability of this system to derive quantitative

95 information on aerosol hygroscopicity, composition, and effective density (Zelenyuk et al.,

96 2008). Herich et al. firstly applied the tandem HTDMA-ATOFMS system to characterize

97 particle composition of different hygroscopicity (Herich et al., 2008;Herich et al., 2009). A large

98 portion of the less hygroscopic modes were found to be contributed by organics and combustion

99 species both in the urban and remote site, while the sulfates and nitrates were present in almost

100 all particles independent of hygroscopicity. Similar findings were also observed in our

101 preliminary characterization using HTDMA-ATOFMS in Shanghai city (Wang et al., 2014),

102 except higher nitrate and sulfate intensities were found in hygroscopic particles in our study.

103 However, the preliminary dataset was not sufficiently large since only a few GF were

104 characterized in that study (GF 1.05-1.1, 1.3, 1.4 and 1.5 at 85% RH). The primary objective

105 of the present study is to establish more complete connections between hygroscopicity and

106 single particle signatures, which could be further utilized to predict hygroscopicity of ambient

107 particles. We conducted a comprehensive HTDMA-ATOFMS experiment with the particle GF

108 varied in a more complete range (0.9~1.7, 85% RH), which accounted for the main number

109 fraction of atmospheric particles in urban atmosphere (Liu et al., 2014;Liu et al., 2011;Ye et al.,

110 2013) . Based on the HTDMA-ATOFMS data, we further developed and tested a method to

111 estimate the hygroscopicity of ambient particles analyzed by ATOFMS.

112 ## *2. EXPERIMENTAL SECTION*

113 ### 2.1. HTDMA

114 The custom-built HTDMA (Ye et al., 2009) consists of two DMAs and a humidifier connected

115 in series (Figure 1). Aerosol was dried before entering HTDMA (RH ~10%) by a diffusional

116 silica gel tube. The dried aerosol reached charge equilibrium in a Kr-85 neutralizer. The DMA1

117 (Model 3081, TSI Inc.) selected particles by electrical mobility size as D_{dry}. The monodisperse

118 particles from DMA1 grew in a Nafion humidifier (RH=85%). The sizes of humidified particles

119 D_{RH} was determined by the second DMA connected by a CPC to measure their concentrations.

120 The sheath flow rate in DMA2 (3 l/min) was regulated by mass flow controller. The RH of the

121 DMA2 sheath flow was managed to match the humidifier (85% RH). The HTDMA were

122 installed in thermostatic chamber in which temperature was controlled to $25\pm0.1℃$. The total

123 aerosol flow was 0.4 L/min (the sum flow rate of the CPC, 0.3 L/min and the ATOFMS, 0.1

124 L/min). Aerosol residence time in humidifier was ~10 s. PSL spheres of known size and

125 $(NH_4)_2SO_4$ salt were used to calibrate the HTDMA. The HTDMA uncertainty in GF

126 determination is ±0.05 (Ye et al., 2009;Swietlicki et al., 2008).

127 ### 2.2. ATOFMS

128 The schematic of ATOFMS (Model 3800-100, TSI. Inc) is illustrated in Figure 1. Particles were

129 drawn into ATOFMS through a 0.1mm orifice and focused into narrow beam through

130 successive expansions and contractions in the aerodynamic focusing Lens (AFL). Particles

131 leaving the AFL obtain velocities depending on their aerodynamic sizes. In the ATOFMS sizing

132 region particles pass through two orthogonally oriented continuous lasers (Nd: YAG, 532 nm)

133 and laser light was scattered. The scattered light generates pulses in two photomultiplier tubes

(PMT) and the signal delay between the two pulses is used to calculate particle velocity. Particle velocity was also used to trigger ionization laser (Nd: YAG, 266 nm) at exact time to ionize particles. The negative and positive ions generated from particles are recorded by a dual polar time-of-flight mass spectrometer. More details of ATOFMS were described elsewhere (Su et al., 2004).

The ATOFMS data was analyzed within the YAADA toolkit (http://www.yaada.org/). Particles showing similar composition were classified by the adaptive resonance theory-based clustering algorithm (ART-2a) (Song et al., 1999). The ART-2a algorithm parameters were set to: vigilance factor = 0.85, learning rate = 0.05 and number of iterations = 20. The clusters generated by the ART-2a were manully regrouped into major types by considering their common composition patterns. The obtained particle types were labelled by refering to previous single particle characterization studies (Spencer et al., 2006;Silva et al., 1999;Sullivan et al., 2007;Gaston et al., 2011;Qin et al., 2012).

2.3. Sampling description

The HTDMA-ATOFMS characterization was carried out at the building of department of environmental science and technology in Fudan university (31°18'N, 121°29'E) from Feb-26 to Mar-7, 2014. Aerosol inlet was installed at the building roof about 6 m above the ground. The Fudan campus was influenced by local emissions sources from transportation, residential, business and cooking activities from surrounding areas which can be viewed as urban environment. A period of ambient ATOFMS data, which persisted from Sep-12 to Sep-28, 2012, was recorded at the same site in Fudan campus. Ambient air quality data of pollutants concentrations ($PM_{2.5}$, O_3, and SO_2) in Shanghai city were provided by Shanghai Environmental Monitoring Center (SEMC).

The sampling procedure was similar to our previous study (Wang et al., 2014). The typical HTDMA GF distributions in this site showed two separated hygroscopicity modes. In 85% RH condition, the two modes were present with respective center GF of 1.05 and 1.45, which were conventionally classified as Near-Hydrophobic (NH) and More-Hygroscopic (MH) modes, respectively (Swietlicki et al., 2008). These modes were normally present elsewhere in China

162 and other areas (Liu et al., 2011;Swietlicki et al., 2008). The HTDMA data suggest that the

163 majority of particles (>97 %) were of GF in 0.9-1.7 range. Consequently, particles in this GF

164 range were characterized by HTDMA-ATOFMS with a GF step of 0.1.

165 To characterize the desired GFs, the two DMAs in HTDMA were set at certain diameters D_{dry}

166 and D_{RH} according to GF=D_{RH}/D_{dry}. The HTDMA-ATOFMS system was kept sampling until a

167 sufficient number of particles (> 200) were analyzed by ATOFMS for each GF setting (Table

168 1). We fixed the DMA1 (D_{dry}) diameter to 250 nm, while the DMA2 diameter (D_{RH}) was set as

169 shown in Table 1. The number of particle spectra in ATOFMS was affected by ambient particle

170 concentrations of certain GF. Since particle concentrations in the downstream of HTDMA were

171 very low, longer sampling were maintained to record sufficient number of spectra in ATOFMS

172 (See the CPC concentrations in Figure S1). The ATOFMS instrument used in this study has size

173 detection range of 100-3000 nm. Considering this, the detection efficiency for 250 nm is

174 expected to be low, as 250 nm is on the lower end of ATOFMS detection range. However, in

175 HTDMA-ATOFMS experiment we selected 250 nm particles, because the concentrations of

176 larger particles were found to decrease further in SMPS size distributions. Therefore, the

177 selection of D_{dry} as 250 nm is a compromise between detection efficiency and particle

178 concentrations (Wang et al., 2014;Herich et al., 2008). With the measured ATOFMS particle

179 numbers and CPC concentrations, the detection efficiency of ATOFMS were calculated to be

180 ~1.6×10^{-2} at the dry size. In Figure S2 we presented ATOFMS detection efficiencies together

181 with the particle hit rate (hit particles/total sized particles) at different growth factors. Generally,

182 the detection efficiencies suggested variations at different GFs. We found higher detection

183 efficiencies in moderate GF range (1.2-1.4) and higher hit rates in GF<1.3 range, which is

184 probably caused by variations of compositions with GF (Hatch et al., 2014).

185 **2.4. Estimation of ambient particle hygroscopicity**

186 Particles in HTDMA-ATOFMS dataset is comparable to ambient ATOFMS particles. Particle

187 types typically present in HTDMA-ATOFMS study were also preset in ambient ATOFMS

188 studies. Therefore, it is possible to assign similar GF to ambient particles if they have similar

189 composition. The estimation method was firstly performed by evaluating spectra similarities

190 between ATOFMS and HTDMA-ATOFMS dataset (dot products of normalized spectra). The

191   ATOFMS is known to have higher detection efficiencies toward some metals (such as Na, K,

192   Fe), resulting inappropriately large peaks in particle spectra. We solved the bias by taking the

193   0.5 power treatment to peaks intensities (Rehbein et al., 2012). In this treatment the larger peaks

194   were suppressed in some degree while smaller peaks increased their weigh relatively. The 0.5

195   power treatment to peaks intensity was applied because it offered better results in the estimation

196   of hygroscopicity than without it, as discussed in the supplemental information (Figure S3). In

197   the second step we searched matched particles from the HTDMA-ATOFMS dataset showing

198   the best similarities with the ambient particle (dot products in 95-100% range of the maximum

199   dot product). In this study we set a threshold similarity (0.7 dot product) in matching particles,

200   as was required in ART-2a algorithm (Song et al., 1999). Ambient particles with matching dot

201   products <0.7 were excluded from analysis of the estimated GF. The similarity data suggests

202   that 96.2% of the matching similarities are > 0.7 and 79% of them are >0.8 (Figure S4). Since

203   each of the matched particles in HTDMA-ATOFMS dataset was associated with a GF, we

204   obtained a collection of the matching GFs (0.9 -1.7 in 0.1 step). The estimated GF of the

205   ambient particle was determined to be the weighted average of the matched GFs, with the

206   weights being the number percentage of matched particles in each GF bins:

207    $$GF_{pred} = \frac{\sum GF_i \cdot F_i}{\sum F_i}$$

208   where: GF_{pred} = the estimated GF of ambient particle, GF_i = GF value from 0.9 to 1.7

209   interspaced by 0.1, F_i = number percentages of the matched particles in each GF bin.

210   The estimation process relied on statistical approach in estimating the most probable

211   hygroscopicity for ambient particles, rather than by inferring particle compositions of single

212   particles (Healy et al., 2014). The latter method derived quantitative concentrations of various

213   compositions from peak intensities, which were then applied to predict particle hygroscopicity

214   using the Zdanovskii-Stokes-Robinson mixing rules. Some assumptions including material

215   densities were needed in that method. As a comparison, we inferred hygroscopicity by matching

216   particles with HTDMA-ATOFMS particles of known hygroscopicity. Therefore, the estimated

217   GFs were derived from the measured GF and the assumptions of composition densities and

218   detection sensitivities in ATOFMS are obviated.

219 The uncertainties in the GF prediction in this method were estimated. The uncertainties in

220 eventual GF may stem from the intrinsic uncertainties in HTDMA-ATOFMS techniques. For

221 the estimation algorithm itself, only few parameters exist that are capable to affect the estimated

222 GF. With the 0.5 power treatment to peak intensities, the only parameter that could influence

223 the estimated GF would be the matching criteria of particles. We have adjusted the matching

224 criteria of 95-100% maximum dot products to 90-100% and 98-100% and the variations in

225 particle GFs were inspected (Figure S5). Based on the variations of the obtained GF, we

226 estimated that the uncertainty in GF estimation is within ± 0.15.

227 ### *3. RESULTS AND DISCUSSIONS*

228 **3.1. Single particle composition and hygroscopicity in HTDMA-ATOFMS experiment**

229 **3.1.1 Hygroscopicity distribution of different particle types**

230 The particles in the HTDMA-ATOFMS dataset were classified into major types based on their

231 mass spectra. The ART-2a algorithm was applied to particle clustering and then similar clusters

232 were combined. The majority of particles were eventually classified into 9 types including

233 Biomass, Fresh EC, Aged EC, Dust/Ash, HMOC, Amine-rich, Ammonium/OC, Cooking and

234 Sea salt. In Figure 2 we present the average spectra of each type and their numbers detected in

235 each GF bin. Since the total number of detected particles in GF bins were not equal (Table 1),

236 we also present the particle numbers normalized by the total numbers to indicate their detection

237 probability in each GF bin (Figure. 2). The hygroscopicity of particle types showed different

238 distribution patterns with GF. The hygroscopicity characters of Biomass, EC, Dust/ash, HMOC

239 and Amine-rich types were described previously and their hygroscopicity have shown

240 consistent trend with the previous characterization (Wang et al., 2014).

241 The Biomass particles produced characteristic peaks of -26(CN), -42(CNO), -59($C_2H_3O_2$), -

242 73($C_3H_5O_2$) and dominant peak at 39K and related peaks at 113(K_2Cl) or 213(K_3SO_4) (Silva et

243 al., 1999;Zauscher et al., 2013;Pratt and Prather, 2009). Biomass particles displayed low

244 hygroscopicity since majority of them were present in GF <1.2 range, with the peak detection

245 probability at GF 1.1 (Figure 2 (a)). The hygroscopicity of Biomass particles is consistent with

246 other HTDMA measurement of biomass particles (Rissler et al., 2006;Laborde et al., 2013).

247   The hygroscopicity of biomass particles in ambient environment were similarly detected in the

248   HTDMA-SP2, which suggested the center GF of 1.1~1.2 of biomass particles (at 90% RH),

249   corresponding to the GF of 1.06-1.13 at 85% RH (Laborde et al., 2013).

250   The EC particles were detected by a series of elemental carbon peaks at C_n (n=1, 2, 3 …) in the

251   negative and positive spectra (Ault et al., 2010;Spencer et al., 2006;Toner et al., 2008). EC

252   particles distributed broadly from nearly-hydrophobic (NH) mode to more-hygroscopic (MH)

253   mode. However, the mass spectra of hydrophobic and hygroscopic EC particles were different

254   in their mass spectra. As shown in Figure 2 (b-c), The mass spectra of hygroscopic EC particles

255   produced stronger secondary peaks ($-62NO_3^-$, $-97HSO_4^-$, $18NH_4^+$) than hydrophobic EC

256   particles, consistent with the significant fractions of secondary matters in hygroscopic EC

257   (Laborde et al., 2013). According to their hygroscopicity distributions, the general EC type was

258   divided into Fresh EC and aged EC type. The mass spectra of Fresh EC suggested they were

259   freshly emitted without significant secondary coatings (Weingartner et al., 1997;Laborde et al.,

260   2013;Herich et al., 2009). Peak intensity trends of $62NO_3^-$, $-97HSO_4^-$, $18NH_4^+$ and other related

261   peaks at different GF were summarized for EC particles (Figure S6). Based on the statistics of

262   peak intensities, we found clear increasing trends of secondary peak intensities in GF 0.9-1.2

263   range, but not in all GFs (Laborde et al., 2013;Herich et al., 2008).

264   Dust/ash type particles produced inorganic peaks of salts and metals (Gaston et al., 2017;Ault

265   et al., 2011;Sullivan et al., 2007). Most of dust/ash particles were detected in hygroscopic range

266   (GF>1.3). Most of Dust/ash particles were internally mixed with nitrate. Within the general

267   Dust/ash type there are many sub-clusters according to specific association of metal peaks in

268   particle spectra. Some of the clusters showed characteristic hygroscopicity distributions which

269   offered values in the source apportionment of these particles. As an illustration, we presented

270   the mass spectra and hygroscopicity distribution of the Al-Si cluster in Figure 3. The mass

271   spectra of Al-Si particles showed stronger aluminum ($27Al^+$) and silicate ($-76SiO_3^-$) peaks in

272   their positive and negative spectra, respectively. Particle number distribution of Al-Si particles

273   suggested that they were detected with the highest probability at GF 1.1. In the preliminary

274   study we identified the similar Al-Si particles exclusively in NH mode (Wang et al., 2014).

275   Based on their hygroscopicity distribution, we assumed the Al-Si particles are soil dusts

276   according to their reported low hygroscopicity (Koehler et al., 2009).

277   The spectra of HMOC particles showed obvious organic peaks in higher m/z range (>150).

278   Some HMOC particles produce obvious polycyclic aromatic hydrocarbons (PAH) peaks in

279   positive spectra and high mass signals in negative spectra. The mass spectra of HMOC

280   suggested they were generated from combustion including traffic emissions (Dall'Osto et al.,

281   2013;Toner et al., 2008). The majority of HMOC particles displayed low hygroscopicity

282   (GF<1.2) (Wang et al., 2014;Herich et al., 2008).

283   Amine-rich type particles produced amine peaks at +59(C_3H_9N), +86($C_5H_{12}N$) and

284   +101($C_6H_{15}N$) (Angelino et al., 2001;Pratt et al., 2009). Particulate amine formation was

285   favored in low temperatures and higher humidity conditions (Huang et al., 2012;Zhang et al.,

286   2012). The elevated amine particle fractions may be related to the low temperature (6 °C) and

287   high humidity (78% RH) condition during this experiment. Both the preliminary and present

288   study identified the hydrophilicity of Amine-rich particles, with the highest number

289   contributions to GF>1.5 range (Wang et al., 2014). Short alkyl chain aliphatic amines are known

290   to have relatively high vapor pressures and basic in nature, their presence in particles indicates

291   they are most likely occur in the form of aminium salts, whose formation is greatly favored in

292   the presence of particulate water (Angelino et al., 2001;Chen et al., 2019). Mass spectra of

293   Amine-rich particles suggest that 77% of them were internally mixed with sulfate or nitrate.

294   With the expanded GF range and sampling durations, we identified other particle types of

295   specific hygroscopic patterns, including Ammonium/OC, Cooking and Sea salt particles in this

296   study. The Ammonium/OC particles demonstrated some similarities with biomass particles.

297   There was predominant potassium peak ^{39}K and many organic peaks in the positive mass

298   spectra, as shown in Figure 2. Additionally, stronger $18NH_4^+$ peaks for ammonium and sulfate

299   (-97HSO_4) were also present in these particles. The typical -26CN^- and -42CNO^- peaks

300   observed for biomass particles were absent or very weak, suggesting the composition

301   differences between Ammonium/OC and biomass particles (Silva et al., 1999;Zauscher et al.,

302   2013;Pratt and Prather, 2009). The hygroscopicity of the Ammonium/OC particles was unique

303   since they have the largest contributions to moderate GF range (GF 1.1-1.3), with the maximum

304   contribution found at GF=1.2. The GF of Ammonium/OC particles suggests that they can be

categorized as LH mode (Swietlicki et al., 2008). A prior ATOFMS study identified that Ammonium/OC particles were from agricultural sources, and found most of them were present in higher photochemical oxidation periods (Qin et al., 2012), consistent with the prominent secondary peaks of ammonium found in this study. It is likely the organics in this type is secondary since the GF 1.2 is close to the hygroscopicity of SOA (GF=1.24 at 90% RH) (Gysel et al., 2007;Sjogren et al., 2008). We inferred that ammonium was not contributing major fractions to Ammonium/OC particles, since ammonium salts was very hydrophilic while Ammonium/OC demonstrate only moderate hygroscopicity.

Cooking is an important source of primary organic aerosol (POA) in urban regions (Crippa et al., 2013;Dall'Osto and Harrison, 2012). Zhang et al. estimated that up to 35% of POA are attributed to cooking aerosol during meal hours (Zhang et al., 2007). Cooking particles around the site was likely to be significant considering that the Fudan campus is located in a heavily populated area. The ATOFMS characterization of cooking particles have been performed previously (Dall'Osto et al., 2013). The marker peaks at -255($C_{16}H_{32}O_2$, palmitic) and -281 ($C_{17}H_{34}O_2$, oleic acid) in the negative spectra were used to identify Cooking particles (Dall'Osto and Harrison, 2012;Silva, 2000). As shown in Figure 2(h), Cooking particles demonstrated very low hygroscopicity and were detected exclusively in GF<1.1 range. It is noted that GF 0.9 does not necessarily indicate a particle shrinkage in 85% RH. Cooking particles might become more spherical in elevated RH, resulting in smaller mobility diameters. This phenomenon was observed for other organic particles (Shi et al., 2012;Pratt and Prather, 2009). The low hygroscopicity of cooking particles is consistent with the enriched organic as indicated by the fatty acids (-171, -255, -279, -281) and HOA (+55, +57) peaks in the spectra. The detection of cooking particles in NH mode complemented to the conclusion that combustion processes are mainly responsible for NH particles (Swietlicki et al., 2008;Laborde et al., 2013;Herich et al., 2009).

With particles of higher GF being analyzed in this experiment, we also identified the Sea salt particle which constitutes an important particle type in ambient air in coastal areas (Herich et al., 2009;Gard et al., 1998). Sea salt mass spectra contain dominant sodium peak $23Na^+$ and other sodium cluster peaks at $62Na_2O^+$, $63Na_2OH^+$, $81Na_2Cl^+$ (Gaston et al., 2017). The

334 hydrophilicity of Sea salt is clear that they were mostly detected in the largest GF bins (>1.5),

335 with their number fractions increased from GF 1.5 to 1.7 (Figure. 2). HTDMA studies in marine

336 environment shown that sea salt particles constitute a separated hygroscopicity mode of the

337 largest GF (Swietlicki et al., 2008), which is generally consistent with the observed GF range

338 in the experiment. However, the observed sea salt particle hygroscopicity is somewhat different

339 from the HTDMA-ATOFMS characterization in a subarctic region, where sea salt particles

340 were found mainly detected in GF 1.3-1.5 range at 82% RH (Herich et al., 2009). We inferred

341 that sea salt hygroscopicity properties are variant with locations and other factors (organics in

342 seawater, marine microbiological conditions, aging) should be considered (Facchini et al.,

343 2008;Randles et al., 2004).

344 **3.1.2 Peak intensity variations with GF**

345 Apart from particle number distributions, the HTDMA-ATOFMS dataset provided another

346 aspect of information regarding peak intensities with GF. In this study, we used relative peak

347 intensities (peak areas normalized by the total areas in spectrum) to investigate its relation to

348 GF. Generally, the responses of peak intensity to GF variation were found to be nonlinear, since

349 they were correlated only within specific GF ranges. A simple trend applicable to whole GF

350 range was not observed.

351 We presented the statistics of peak intensity of nitrate ($46NO_2^-$, $62NO_3^-$, $125H(NO_3)_2^-$) and

352 sulfate ($80SO_3^-$, $97HSO_4^-$) which were known to be critical to particle hygroscopicity (Figure

353 4). As previously observed, the nitrate and sulfate peaks were present in the majority of particles

354 in all GF bins (Herich et al., 2009;Herich et al., 2008;Wang et al., 2014). However, peak

355 intensities of nitrate and sulfate were indeed stronger in hygroscopic particles than hydrophobic

356 particles. In Figure 4 we observed positive correlation between nitrate and sulfate intensities

357 and GF in GF <1.2 range, suggesting contribution of nitrate and sulfate to particle

358 hygroscopicity in low GF range (Figure 4). However, in higher GF range (GF 1.3-1.5), nitrate

359 and sulfate peaks seem to reach a plateau with unclear dependence on GF. Nitrate and sulfate

360 were known to contribute large fractions of particle mass in MH particles (Swietlicki et al.,

361 2008;Laborde et al., 2013;Liu et al., 2014). The unclear trend of nitrate and sulfate with GF

362 seem to suggest that nitrate and sulfate were in stable ratios since nitrate and sulfate peaks were

dominating peak areas in negative spectra. For particles of even higher GF, differences were observed between GF 1.3-1.5 and GF 1.5-1.7 range in that stronger nitrate and weaker sulfate peaks were detected in the GF 1.3-1.5 range. Particles classification suggests that this general characteristic is also at variance for different particle types. The same statistics for EC and Dust/ash particles were presented in Figure 4. Compared with EC particles, smaller sulfate and stronger nitrate peaks were found in Dust/ash spectra, and the observed trend in total particles were less obvious in Dust/ash. These facts highlight the nonlinearity between peak intensities and GF and that particle types should also be considered in describing peak intensities.

The analysis of peak intensities with GF can disclose some atmospheric processes happened on aerosol. We take the Sea salt as an illustration. Sea salt particles were known to react with atmospheric nitric acid, with NaCl in fresh sea salt be transformed into $NaNO_3$ in the reacted sea salt (Gard et al., 1998). This composition transformation is indicated in corresponding changes of NaCl and $NaNO_3$ peak intensities in particle spectra. The unreacted sea salt particles tend to produce larger peaks of Na_2Cl^+ and $NaCl_2^-$ in spectra (Gaston et al., 2011;Prather et al., 2013). In particle spectra of reacted sea salt, the NaCl peaks (Na_2Cl^+, $NaCl_2^-$) decrease while $NaNO_3$ peaks ($Na_2NO_3^+$, $Na(NO_3)_2^-$) increase. We presented peak intensities of sea salt in GF 1.5-1.7 range where sea salt particles were detected with largest numbers (Figure 5). We found that the positive correlation between NaCl peak intensity and GF, and the negative correlation for $NaNO_3$ peaks. Therefore, the HTDMA-ATOFMS data supported that reacted sea salt have reduced hygroscopicity (Herich et al., 2009;Gaston et al., 2018). Laboratory HTDMA study suggested that NaCl and $NaNO_3$ have deliquesced at 85% RH and that the $NaNO_3$ (GF ~1.8) is less hygroscopic than NaCl (GF ~2.2) (Hu et al., 2010). The reduced hygroscopicity of sea salt is in line with the GF of sodium salts. However, the sea salt hygroscopicity (GF 1.5-1.7) was smaller than pure $NaNO_3$ salt (supposing fully reacted), suggested that the chemical transformation alone is not sufficient to account for the observed hygroscopicity of sea salt. We hypothesize that other compositions as organics were mixed into sea salt and contributed to the reduction of sea salt hygroscopicity (Gaston et al., 2011;Randles et al., 2004;Facchini et al., 2008).

3.2 Predictability of hygroscopicity from particle mass spectra

392   The GF of a particle can be estimated based on HTDMA-ATOFMS data for two reasons. First,

393   different particle types had distinct GF distributions. Second, particles in different GF bins had

394   different mass spectra. The GF estimation from particle spectra requires that the HTDMA-

395   ATOFMS data is capable to represent the major particle types normally presented in atmosphere,

396   which is evidenced in the preceding discussions. In another aspect, the GF prediction from mass

397   spectra also demands that HTDMA-ATOFMS data are sensitive to reflect the composition

398   differences with GF variations.

399   To test the sensitivity of HTDMA-ATOFMS data, we evaluated the average spectral similarities

400   between each pair of GF groups. The average similarities were calculated from the similarities

401   between every possible pairs of particles from the two GF groups. The self-comparing of

402   particles within the same GF group were excluded. As shown in Figure S7, we observed a

403   general trend that particles in the same GF bins tend to produce the highest similarities. As the

404   GF differences increase, the mass spectra similarity between two GF bins tended to decrease.

405   This result is an evidence that the particles with different GFs are more likely to have

406   discriminable mass spectra, which suggests that the HTDMA-ATOFMS dataset are capable to

407   estimate hygroscopicity just from particle mass spectra.

3.3 Estimated hygroscopicity of ambient particles

409   A case study of the hygroscopicity estimation were carried out based on a period of ambient

410   ATOFMS measurement. The ATOFMS data was collected at the same Fudan site from Sep-12

411   to Sep-28, 2012. During this period the ATOFMS recorded 538,983 mass spectra of individual

412   particles. With the described estimation method, the GF value (corresponding to 85% RH) was

413   generated for each particle based on individual particle mass spectra. A fraction of the estimated

414   GF (4%) were excluded from analysis since their maximum similarities failed to exceed the

415   threshold value (dot product > 0.7) between ATOFMS and HTDMA-ATOFMS particles.

416   Particle mixing states in this period were analyzed by clustering particles using ART-2a

417   algorithm (Song et al., 1999). After merging the clusters of similar composition and temporal

418   trends, the majority of particles were finally grouped into the same general types as discussed

419   in HTDMA-ATOFMS dataset (Fresh EC, Aged EC, Dust/Ash, HMOC, Amine-rich,

420   Ammonium/OC, Cooking and Sea salt), which account for 90.8% of the total analyzed particles

421   in this period.

422   **3.3.1 Hygroscopicity modes and contributions of particle types**

423   The estimation method determined that the GF of ATOFMS particles were restricted within the

424   GF range in HTDAM-ATOFMS dataset (0.9-1.7). Within this GF range, the ATOFMS particle

425   GF distribution suggested several hygroscopicity modes similar to the HTDMA measurement.

426   As shown in Figure 6, three hygroscopicity modes were clear in the GF-number distributions,

427   with particle GF centered at about 1.05, 1.42, and 1.6, respectively (85% RH). Prior HTDMA

428   studies suggested the regular presence of the nearly-hydrophobic mode with center GF in

429   1.05~1.1 range in Shanghai area (Ye et al., 2011), consistent with the GF 1.05 mode in this

430   study. The second mode at GF 1.42 mode in ATOFMS particles corresponds to the MH mode

431   (GF 1.43~1.47) in Shanghai and other sites using HTDMA (Ye et al., 2013;Ye et al., 2011;Liu

432   et al., 2011). The sea salt mode in HTDMA GF distribution is not always clear because of the

433   larger size of sea salt particles. However, the sea salt particles were readily detected by

434   ATOFMS because of the detection range of ATOFMS. The particles in GF 1.6 mode contained

435   rich sodium content and their mass spectra suggest typical sea salt peaks (Figure S2). In marine

436   areas the sea salt particles were found to constitute hygroscopicity mode of the largest GF

437   (about 2.0 at 90% RH, corresponding to 1.76 at 85% RH) (Swietlicki et al., 2008).

438   The ATOFMS measured particle aerodynamic diameters simultaneously for individual particles.

439   Together with the estimated GF, we inspected particle number distribution as a bivariate

440   function of the estimated GF and diameter (aerodynamic diameter, d_{va}) (Figure 7). The

441   hygroscopicity modes were clearer in the GF-d_{va} diagram, which suggest the increasing trend

442   of particle diameter with increasing GF, a very consistent result with HTDMA studies (Ye et

443   al., 2011;Ye et al., 2013). Healy et.al. applied a different method to estimate particle

444   hygroscopicity from single particle data using ZSR mixing rule (Healy et al., 2014). The particle

445   aerodynamic diameter d_{va} was transformed to equivalent mobility diameter d_m by assuming a

446   particle density in that study. Although the methods are different, the identified hygroscopicity

447   modes were similar between the two studies, except the sea salt mode which was not found by

448   Healy et al. (Healy et al., 2014).

449   Based on the GF of hygroscopicity modes, prior HTDMA studies conventionally classified the

450   observed modes into categories as nearly-hydrophobic (NH), less-hygroscopic (LH), more-

451   hygroscopic (MH) and sea salt (SS) modes respectively (Swietlicki et al., 2008;Liu et al.,

452   2011;Sjogren et al., 2008). However, the chemical nature of these hygroscopicity modes was

453   not clear since the HTDAM technique is based on particle numbers and the particle composition

454   information was not obtainable. With the ATOFMS single particle data, particle composition

455   and hygroscopicity was connected directly. To facilitate comparison, we similarly divide the

456   estimated GF into four bins (<1.1, 1.1-1.3, 1.3-1.5 and >1.5) to roughly represent the NH, LH,

457   MH, SS particles according to the conventional classification of hygroscopicity modes

458   (Swietlicki et al., 2008). As shown in Figure 6, particle types were distributed differently in GF

459   modes. For example, the organic particles including HMOC, Biomass and Freshly emitted EC

460   particles were mainly enriched in NH mode, which suggests directly that combustion sources

461   are mainly responsible for NH particles in the ambient (Herich et al., 2008;Herich et al.,

462   2009;Ye et al., 2011).

463   In Table 2 we made the statistics on average number contributions of particle types to the NH,

464   LH, MH and SS mode. The presented statistics were based on the temporal contributions of

465   each particle types in daily resolution. It is noted that particle number contributions presented

466   in Table 2 may be different from HTDMA-ATOFMS dataset (Figure 2). For example, the

467   Cooking particles contributions to NH mode was significantly lower in the ATOFMS dataset

468   (3%) than HTDMA-ATOFMS dataset (19%). This result is understandable because particle

469   concentrations are variant with particle size and HTDMA-ATOFMS only analyzed a narrow

470   size bin from the total particle size distribution. For each hygroscopicity mode, there were

471   multiple particle types contributing significant number fractions, suggesting that even within

472   the same hygroscopicity mode there were still some heterogeneity in particle composition.

473   Particles in the same hygroscopicity mode may share some common features in compositions

474   but their differences are distinguishable in single particle data. In another respect, the

475   contributions of each type also suggest the existence of a predominant type that accounts for

476   major fractions in respective modes compared with other types, such as Aged EC in MH mode,

477   Ammonium/OC in LH mode. The comparison between Table 2 and Figure 2 suggests that,

although their absolute contributions may be different, the hygroscopicity patterns of particle types in the two datasets are in good agreement. Based on this fact, we concluded that the composition-hygroscopicity connections contained in HTDMA-ATOFMS dataset was successfully reflected into the predicted GF.

3.3.2. Temporal variations of estimated hygroscopicity

The temporal variation of particle estimated GF from Sep-12 to Sep-28 was illustrated in Figure 8. Four distinct periods (P1-P4) were identified based on their different hygroscopicity distributions. Generally, the P1 and P3 periods were characterized by elevated MH mode which dominated the ATOFMS particles numbers, while in P2 and P4 the MH particles decreased significantly and sea salt mode was pronounced. Back trajectories during P1-P4 were analyzed using HYSPLIT mode (Draxler, R. R. and Rolph, G. D., 2003) to inspect the airmass that influenced the sampling site (Figure S9). The 24-hour back trajectories suggests that the airmass in P1 period mainly circulated in local regions from northwest direction to Shanghai. The local circulations brought regional aerosol pollution to the sampling site, resulted in elevated concentrations of particles, especially the MH particles. During P2, the airmass originated from the ocean in northeast direction with less continental influence. The cleaner air from the ocean almost wiped out the accumulated particles observed in P1 and the concentrations of sea salt particles increased. In the majority of time during P3, the airmass stayed over continental areas. The MH particles dominated particle numbers in this period and the sea salt mode were barely present. During Sep-18 to Sep-20 in P3, the LH particles showed increased concentrations and gradually decreased after Sep-20. Similar to P1, the origin of airmass in P4 shifted to the ocean in eastern directions and SS mode emerged again. Both the particle spectra and the back trajectories supported that the GF mode of 1.6 can be mainly attributed to sea salt particles.

Except meteorological conditions, other differences exist in the temporal trends for each hygroscopicity modes. Generally, the NH mode showed relatively stable trends irrespective of different periods of P1-P4, as indicated in Figure 8. Closer inspection of NH particles suggests a notable feature that obvious sharp spikes were present in NH particle temporal concentrations (Figure 8). This character is typical for particles from local emission sources, with undissipated plumes at the time of detection. With the combined information from particle composition in

507   Table 2, we inferred that the NH particles were fresh emitted particles from local sources with

508   high organic or elemental carbon content (Laborde et al., 2013;Herich et al., 2008;Weingartner

509   et al., 1997). The mass spectra of NH particles indicated low nitrate and sulfate signals,

510   suggesting that secondary matters have not accumulated significantly on these particles,

511   consistent with negligible coating thickness on NH particles (Laborde et al., 2013). We tend to

512   ascribe the organics in NH particles to be primary organic carbons (POA) considering their

513   relatively fresh emission state (Sjogren et al., 2008;Liu et al., 2011;Gysel et al., 2007).

514   Some characters of LH particles were noticed. Similar to the particles in MH range, the LH

515   particles mainly presented in continent influenced periods (P1 and P3) (Figure 8). However, the

516   temporal concentrations trends suggested differences between LH and MH particles. For

517   example, MH mode dominated particle numbers in the entire P3, while the LH particles were

518   only pronounced from Sep-17 to Sep-21, with peak concentrations observed on Sep-19. The

519   particle contributions showed that Ammonium/OC is the main contributor to NH particles

520   (Table 2). This conclusion is also correct in temporal basis since the Ammonium/OC

521   contributions to LH range were always much larger than other types of particles in all the

522   studied period. We investigated the nature of the Ammonium/OC particles by comparing its

523   concentration with ambient pollutants levels. As shown in Figure 9, the number fractions of

524   Ammonium/OC particles showed strong connections to ambient O_3 concentrations. During

525   Sep-17 to Sep-21 there were daily oscillations of O_3 levels, which were followed by the same

526   pattern of Ammonium/OC particles with lags of several hours. The maximum O_3 concentrations

527   was found on Sep-19 (219 μgm^{-3}) in the period, the same day when the highest Ammonium/OC

528   particle contribution was observed. HTDMA studies suggested that LH mode became

529   pronounced in new particle formation (NPF) periods with high atmospheric reactivity

530   (Swietlicki et al., 2008). Based on these facts, we think the Ammonium/OC particles were

531   related to the oxidation processes of organics vapors by oxidants such as O_3 (Varutbangkul et

532   al., 2006). The moderate hygroscopicity of Ammonium/OC agrees with the hygroscopicity of

533   ambient secondary organic aerosol (SOA) (Gysel et al., 2007;Sjogren et al., 2008). During

534   periods of higher Ammonium/OC contributions (Sep-17 to Sep-21), increased SO_2 levels were

535   also encountered, which coincided with high sulfate signals in mass spectra of Ammonium/OC

536 (Figure 2). Compared with the organic compositions, the sulfate was inferred to have minor

537 contributions to mass fractions because of the moderate hygroscopicity of Ammonium/OC.

538 Particles in MH mode dominated the particle numbers for the majority of time in P1 and P3

539 (60%) compared with the average fraction of 25% in P2 and P4. Inspection of the temporal

540 trends of MH particles also suggest some diurnal variations with higher concentrations in

541 nighttime (Figure 8). As illustrated in Figure 4 and Figure S6, mass spectra of MH particles

542 were dominated by sulfate, nitrate peaks, suggested that MH particles were mixed with

543 significant fraction of secondary inorganic matters (SIA). The coating thickness of the

544 secondary matters was determined by HTDAM-SP2 at different GF (Laborde et al., 2013). The

545 coating thickness of secondary coating was measured to 40-80 nm (D_{dry}=265 nm) in GF 1.2-

546 1.7 range, being equivalent to 55-76% of hygroscopic particle volume was attributed to

547 secondary matters (Laborde et al., 2013;Healy et al., 2014).

548 ### 3.3.3 Peak intensity variations with estimated GF

549 Particle hygroscopicity and peak intensities in particle mass spectra were correlated to show

550 their connections. The correlation was illustrated similarly to the analysis of the HTDMA-

551 ATOFMS dataset, as shown in Figure 10. In addition to the statistics on peak intensities of

552 different GF, the number distributions ATOFMS particles with GF and peak intensities were

553 presented for nitrate ($46NO_2^-$, $62NO_3^-$, $125H(NO_3)_2^-$) and sulfate peaks ($80SO_3^-$, $97HSO_4^-$,) in

554 the lower panels in Figure 10. The general trends of peak intensities with GF in HTDMA-

555 ATOFMS dataset was preserved in estimated GF of ambient particles. The trends of nitrate and

556 sulfate peak intensities showed increases from NH to LH range and remained constant in the

557 MH mode. Similar to HTDMA-ATOFMS particles, stronger nitrate peaks were detected in SS

558 particles compared with the MH particles, while an opposite trend was observed for sulfate

559 intensities. These results highlight the nonlinearity between GF and peak intensities of

560 ATOFMS particles.

561 The nonlinearity of peak intensities with GF was also suggested by the different particle types

562 presented in ATOFMS data. As shown in the lower panels in Figure 10, the distribution of

563 ATOFMS individual particles showed enrichment in different areas in the GF-peak intensity

564   diagram, suggesting the presence of particle groups of different compositions. To illustrate this

565   character, we selected two areas with clear particle enrichments in GF-peak intensity diagram

566   and their particle composition were analyzed (denoted as A and B in lower left panel in Figure

567   10). Obviously, particles in area A produced much larger nitrate signals than particles in area B.

568   Particle numbers in the two areas suggested that Dust/ash dominated particles in area A (59%)

569   while in area B the Dust/ash only accounted for 14% of particles (Figure S10). As a contrast,

570   particles in area B were dominated by Aged EC type (53%) followed by 25% Dust/ash. Table

571   2 suggests that Aged EC and Dust/ash are the major types presented in the same MH mode.

572   However, peak intensity responses to GF were indeed different for different particle types,

573   suggesting the importance of particle types in describing peak intensities.

574   The particle distribution with sulfate intensities showed similar enrichment patterns to nitrate

575   (lower right panel in Figure 11). Sulfate peak intensities were found to correlated with

576   hygroscopicity in GF <1.2 range but in MH range no correlated with GF was observed. We note

577   that except the larger peaks of nitrate and sulfate, some smaller peaks were also found to

578   correlated with GF within specific particle type. We correlated peak intensities of Na_2Cl^+ and

579   NO_3^- with the estimated GF of sea salt particles (Figure S11). The Na_2Cl^+ peaks were positively

580   correlated with GF while the nitrate peaks were negatively correlated with GF. The observed

581   correlation in sea salt particles are consistent with discussed trends in the HTDMA-ATOFMS

582   dataset. These results demonstrate that the GF estimation method have effectively reflected the

583   minor changes in particle mass spectra into the estimated hygroscopicity.

584   **3.3.4 Comparing the estimated hygroscopicity with visibility**

585   Particle optical properties were closely connected to hygroscopicity (Liu et al., 2012;Qu et al.,

586   2015;Chen et al., 2012). The hygroscopic growth increases particle volumes and cross sections

587   and is contributing to the visibility degradation. With the estimated hygroscopicity of ATOFMS

588   particles, we correlated atmospheric visibility with particle concentrations to study their

589   contributions to the visibility variations. The ATOFMS particle volume concentrations were

590   calculated for hygroscopicity modes of NH, LH, MH and SS based on ATOFMS particle

591   diameter and numbers. The particle volume concentrations was used because hygroscopic

592   growth change particle sizes rather than numbers (Chen et al., 2012). The visibility data was

593   obtained from (https://www.wunderground.com/) logged in the Hongqiao airport (31°12' N,

594   121°20' E) and Pudong airport (31°9.3' N, 121°49' E) during the study period (see the map in

595   Figure S12). The temporal variations of visibility in two sites correlated strongly (Figure S12),

596   despite the 45 kilometers distance between two airports. The Fudan site is located roughly

597   between the two airports, and the two sets of visibility data were averaged to represent the study

598   site. In P2 and P4 the site was under the influences from ocean, resulting visibilities larger than

599   10 km (Figure 8). Apart from ATOFMS particles, contemporary $PM_{2.5}$ volume concentrations

600   were also correlated with visibility. The $PM_{2.5}$ volume concentrations were derived from $PM_{2.5}$

601   mass concentrations using particle density (1.4 gcm^{-3}). A strong correlation between ATOFMS

602   particle numbers and $PM_{2.5}$ was found (R^2=0.80).

603   An exponential relation between visibility and PM concentrations was found by the previous

604   study (Qu et al., 2015). After applying the exponential fitting to the visibility and particle

605   volume concentrations, we found a moderate correlation for ATOFMS particles (R^2=0.45) and

606   better correlations for $PM_{2.5}$ concentrations (R^2=0.64) (Figure S13). However, the fitting errors

607   were clearly dependent on ambient RH, with larger errors in higher humidity, indicating that

608   hygroscopicity might affect visibility degradations, which were consistent with other studies

609   (Chen et al., 2012;Liu et al., 2012). To further examine the effect of particle hygroscopicity on

610   visibility, we derived particle volumes in different RH using estimated κ values (Petters and

611   Kreidenweis, 2007). The κ values were calculated using the GF of individual particles at 85%

612   RH for ATOFMS data and the average GF of 1.36 for $PM_{2.5}$ volume concentrations. With

613   hygroscopicity being considered, we found notable improvements of the correlations between

614   PM concentrations and visibility, with the improved correlation observed for $PM_{2.5}$

615   concentrations (R^2=0.82) after applying correction for hygroscopicity (Figure 11). However,

616   this improvement was barely the case for NH particles, probably due to the negligible

617   hygroscopic growth. For the ATOFMS particles in different GF modes, we found the highest

618   R^2 (0.65) for the MH particles. The correlation between SS particles and visibility was distorted

619   due to the visibility reached its limit (10 km) when sea salt mode was pronounced (Figure 8).

620   The R^2 between MH particles and visibility suggests that the variation of MH particles

621   accounted for the major part of visibility changes (65%) during this period, which coincided

622 with the major contribution of nitrate and sulfate to light extinction (61%) in eastern China

623 areas (Qu et al., 2015). These results indicate the importance of discriminating particles by

624 hygroscopicity in explaining the measured visibility.

625 ### *4. CONCLUSIONS*

626 The hygroscopicity and composition of submicron particles were characterized in a megacity

627 in eastern China. A single particle mass spectrometer was connected to the downflow of an

628 HTDMA to analyze particle composition of different hygroscopicity at 85% RH. Direct

629 connections between hygroscopicity and single particle signatures were established. The

630 HTDMA-ATOFMS dataset suggested that particle types were distributed differently in various

631 hygroscopicity ranges. Generally, Fresh EC particles and organic particle types including

632 Biomass, Cooking and high molecular organic carbon (HMOC) were enriched in nearly-

633 hydrophobic (NH) mode (GF<1.1). The majority of particles in NH mode suggested characters

634 of freshly emitted particles from combustion sources. Particle types in the more-hygroscopic

635 (MH) range (GF1.3-1.5) include Aged EC, Amine-rich and Dust/ash particles. The mass spectra

636 of MH particles suggested that they were mixed with significant fractions of secondary matters.

637 The sea salt particles were detected in the higher GF range (GF 1.5-1.7), with increasing

638 detection probability at larger GF. In the moderate hygroscopicity range (GF 1.1-1.3), the

639 Ammonium/OC particles was identified with peak detection probability at GF 1.2.

640 Single particle spectra peak intensities were correlated with GF to disclose their possible

641 connections. The peak intensities were nonlinearly correlated with GF. The peak intensities of

642 nitrate and sulfate showed gradual increase from GF 0.9 to 1.2 while in larger GF range the

643 same trends were not observed. Peak intensities showed opposite directions for nitrate and

644 sulfate in GF 1.5-1.7 range with stronger nitrate peaks and smaller sulfate peaks. Except the

645 general nonlinearity of peak intensities is subjected to variations with different particle types.

646 The peak intensity analysis suggested the reduced hygroscopicity of sea salt after atmospheric

647 aging.

648 Based on the established connections between composition and composition, we developed a

649 method to estimate particle hygroscopicity from single particle mass spectra. The method was

650 tested in a period of ATOFMS data in Shanghai. The estimated GF of individual particles

651 suggested that ATOFMS particles were present in similar hygroscopicity modes as HTDMA

652 measurement on ambient aerosol. We discriminated particles into NH, LH, MH and SS mode

653 by the GF of individual particles. Particle type contributions to the these hygroscopicity modes

654 suggested consistent results with HTDMA-ATOFMS dataset. Based on the combined

655 information on particle composition, hygroscopicity and airmass back trajectories, we inferred

656 that the POA/EC, SOA, SIA and salts are the characteristic compositions for particles in the

657 NH, LH, MH, SS modes, respectively. The proposed method is a novel way of single particle

658 mass spectrometry data analysis, which would provide additional information to the study of

659 particle mixing states, source identification and visibility degradation.

660

REFERENCES

Angelino, S., Suess, D. T., and Prather, K. A.: Formation of aerosol particles from reactions of secondary and tertiary alkylamines: Characterization by aerosol time-of-flight mass spectrometry, Environmental Science & Technology, 35, 3130-3138, 10.1021/es0015444, 2001.

Ault, A. P., Gaston, C. J., Wang, Y., Dominguez, G., Thiemens, M. H., and Prather, K. A.: Characterization of the Single Particle Mixing State of Individual Ship Plume Events Measured at the Port of Los Angeles, Environmental Science & Technology, 44, 1954-1961, 10.1021/es902985h, 2010.

Ault, A. P., Williams, C. R., White, A. B., Neiman, P. J., Creamean, J. M., Gaston, C. J., Ralph, F. M., and Prather, K. A.: Detection of Asian dust in California orographic precipitation, Journal of Geophysical Research-Atmospheres, 116, 10.1029/2010jd015351, 2011.

Buzorius, G., Zelenyuk, A., Brechtel, F., and Imre, D.: Simultaneous determination of individual ambient particle size, hygroscopicity and composition, Geophysical Research Letters, 29, 1974, 10.1029/2001gl014221, 2002.

Chen, J., Zhao, C. S., Ma, N., Liu, P. F., Gobel, T., Hallbauer, E., Deng, Z. Z., Ran, L., Xu, W. Y., Liang, Z., Liu, H. J., Yan, P., Zhou, X. J., and Wiedensohler, A.: A parameterization of low visibilities for hazy days in the North China Plain, Atmospheric Chemistry and Physics, 12, 4935-4950, 10.5194/acp-12-4935-2012, 2012.

Chen, Y., Tian, M., Huang, R.-J., Shi, G., Wang, H., Peng, C., Cao, J., Wang, Q., Zhang, S., Guo, D., Zhang, L., and Yang, F.: Characterization of urban amine-containing particles in southwestern China: seasonal variation, source, and processing, Atmospheric Chemistry and Physics, 19, 3245-3255, 10.5194/acp-19-3245-2019, 2019.

Cheng, Y. F., Wiedensohler, A., Eichler, H., Heintzenberg, J., Tesche, M., Ansmann, A., Wendisch, M., Su, H., Althausen, D., Herrmann, H., Gnauk, T., Bruggemann, E., Hu, M., and Zhang, Y. H.: Relative humidity dependence of aerosol optical properties and direct radiative forcing in the surface boundary layer at Xinken in Pearl River Delta of China: An observation based numerical study, Atmospheric Environment, 42, 6373-6397, 10.1016/j.atmosenv.2008.04.009, 2008.

Crippa, M., DeCarlo, P. F., Slowik, J. G., Mohr, C., Heringa, M. F., Chirico, R., Poulain, L., Freutel, F., Sciare, J., Cozic, J., Di Marco, C. F., Elsasser, M., Nicolas, J. B., Marchand, N., Abidi, E., Wiedensohler, A., Drewnick, F., Schneider, J., Borrmann, S., Nemitz, E., Zimmermann, R., Jaffrezo, J. L., Prevot, A. S. H., and Baltensperger, U.: Wintertime aerosol chemical composition and source apportionment of the organic fraction in the metropolitan area of Paris, Atmospheric Chemistry and Physics, 13, 961-981, 10.5194/acp-13-961-2013, 2013.

Dall'Osto, M., and Harrison, R. M.: Urban organic aerosols measured by single particle mass spectrometry in the megacity of London, Atmospheric Chemistry and Physics, 12, 4127-4142, 10.5194/acp-12-4127-2012, 2012.

Dall'Osto, M., Ovadnevaite, J., Ceburnis, D., Martin, D., Healy, R. M., O'Connor, I. P., Kourtchev, I., Sodeau, J. R., Wenger, J. C., and O'Dowd, C.: Characterization of urban aerosol in Cork city (Ireland) using aerosol mass spectrometry, Atmos. Chem. Phys., 13, 4997-5015, 10.5194/acp-13-4997-2013, 2013.

Draxler, R. R. and Rolph, G. D., HYSPLIT (Hybrid Single-Particle Lagrangian Integrated Trajectory) model v 4.9, NOAA Air Resource Laboratory, Silver Spring MD, available at:

http://www. arl.noaa.gov/ready/hysplit4.html, 2019.

Facchini, M. C., Mircea, M., Fuzzi, S., and Charlson, R. J.: Cloud albedo enhancement by surface-active organic solutes in growing droplets, Nature, 401, 257-259, 10.1038/45758, 1999.

Facchini, M. C., Rinaldi, M., Decesari, S., Carbone, C., Finessi, E., Mircea, M., Fuzzi, S., Ceburnis, D., Flanagan, R., and Nilsson, E. D.: Primary submicron marine aerosol dominated by insoluble organic colloids and aggregates, Geophysical Research Letters, 35, 2008.

Gard, E. E., Kleeman, M. J., Gross, D. S., Hughes, L. S., Allen, J. O., Morrical, B. D., Fergenson, D. P., Dienes, T., Galli, M. E., Johnson, R. J., Cass, G. R., and Prather, K. A.: Direct observation of heterogeneous chemistry in the atmosphere, Science, 279, 1184-1187, 10.1126/science.279.5354.1184, 1998.

Gaston, C. J., Furutani, H., Guazzotti, S. A., Coffee, K. R., Bates, T. S., Quinn, P. K., Aluwihare, L. I., Mitchell, B. G., and Prather, K. A.: Unique ocean-derived particles serve as a proxy for changes in ocean chemistry, Journal of Geophysical Research: Atmospheres, 116, 10.1029/2010jd015289, 2011.

Gaston, C. J., Pratt, K. A., Suski, K. J., May, N. W., Gill, T. E., and Prather, K. A.: Laboratory Studies of the Cloud Droplet Activation Properties and Corresponding Chemistry of Saline Playa Dust, Environmental Science & Technology, 51, 1348-1356, 10.1021/acs.est.6b04487, 2017.

Gaston, C. J., Cahill, J. F., Collins, D. B., Suski, K. J., Ge, J. Y., Barkley, A. E., and Prather, K. A.: The Cloud Nucleating Properties and Mixing State of Marine Aerosols Sampled along the Southern California Coast, Atmosphere, 9, 52, 2018.

Gysel, M., Crosier, J., Topping, D. O., Whitehead, J. D., Bower, K. N., Cubison, M. J., Williams, P. I., Flynn, M. J., McFiggans, G. B., and Coe, H.: Closure study between chemical composition and hygroscopic growth of aerosol particles during TORCH2, Atmospheric Chemistry and Physics, 7, 6131-6144, 2007.

Hatch, L. E., Pratt, K. A., Huffman, J. A., Jimenez, J. L., and Prather, K. A.: Impacts of Aerosol Aging on Laser Desorption/Ionization in Single-Particle Mass Spectrometers, Aerosol Science and Technology, 48, 1050-1058, 10.1080/02786826.2014.955907, 2014.

Healy, R. M., Evans, G. J., Murphy, M., Juranyi, Z., Tritscher, T., Laborde, M., Weingartner, E., Gysel, M., Poulain, L., Kamilli, K. A., Wiedensohler, A., O'Connor, I. P., McGillicuddy, E., Sodeau, J. R., and Wenger, J. C.: Predicting hygroscopic growth using single particle chemical composition estimates, Journal of Geophysical Research-Atmospheres, 119, 9567-9577, 10.1002/2014jd021888, 2014.

Herich, H., Kammermann, L., Gysel, M., Weingartner, E., Baltensperger, U., Lohmann, U., and Cziczo, D. J.: In situ determination of atmospheric aerosol composition as a function of hygroscopic growth, Journal of Geophysical Research-Atmospheres, 113, D16213, 10.1029/2008jd009954, 2008.

Herich, H., Kammermann, L., Friedman, B., Gross, D. S., Weingartner, E., Lohmann, U., Spichtinger, P., Gysel, M., Baltensperger, U., and Cziczo, D. J.: Subarctic atmospheric aerosol composition: 2. Hygroscopic growth properties, Journal of Geophysical Research-Atmospheres, 114, D13204, 10.1029/2008jd011574, 2009.

Hu, D., Qiao, L., Chen, J., Ye, X., Yang, X., Cheng, T., and Fang, W.: Hygroscopicity of Inorganic Aerosols: Size and Relative Humidity Effects on the Growth Factor, Aerosol and Air Quality Research, 10, 255-264, 10.4209/aaqr.2009.12.0076, 2010.

Huang, Y., Chen, H., Wang, L., Yang, X., and Chen, J.: Single particle analysis of amines in ambient aerosol in Shanghai, Environmental Chemistry, 9, 202-210, 10.1071/en11145, 2012.

Koehler, K. A., Kreidenweis, S. M., DeMott, P. J., Petters, M. D., Prenni, A. J., and Carrico, C. M.: Hygroscopicity and cloud droplet activation of mineral dust aerosol, Geophysical Research Letters, 36, L08805, 10.1029/2009gl037348, 2009.

Laborde, M., Crippa, M., Tritscher, T., Juranyi, Z., Decarlo, P. F., Temime-Roussel, B., Marchand, N., Eckhardt, S., Stohl, A., Baltensperger, U., Prevot, A. S. H., Weingartner, E., and Gysel, M.: Black carbon physical properties and mixing state in the European megacity Paris, Atmospheric Chemistry and Physics, 13, 5831-5856, 10.5194/acp-13-5831-2013, 2013.

Liu, H. J., Zhao, C. S., Nekat, B., Ma, N., Wiedensohler, A., van Pinxteren, D., Spindler, G., Muller, K., and Herrmann, H.: Aerosol hygroscopicity derived from size-segregated chemical composition and its parameterization in the North China Plain, Atmospheric Chemistry and Physics, 14, 2525-2539, 10.5194/acp-14-2525-2014, 2014.

Liu, P. F., Zhao, C. S., Gobel, T., Hallbauer, E., Nowak, A., Ran, L., Xu, W. Y., Deng, Z. Z., Ma, N., Mildenberger, K., Henning, S., Stratmann, F., and Wiedensohler, A.: Hygroscopic properties of aerosol particles at high relative humidity and their diurnal variations in the North China Plain, Atmospheric Chemistry and Physics, 11, 3479-3494, 10.5194/acp-11-3479-2011, 2011.

Liu, X. G., Zhang, Y. H., Cheng, Y. F., Hu, M., and Han, T. T.: Aerosol hygroscopicity and its impact on atmospheric visibility and radiative forcing in Guangzhou during the 2006 PRIDE-PRD campaign, Atmospheric Environment, 60, 59-67, 10.1016/j.atmosenv.2012.06.016, 2012.

Lohmann, U., and Feichter, J.: Global indirect aerosol effects: a review, Atmospheric Chemistry and Physics, 5, 715-737, 2005.

Petters, M. D., and Kreidenweis, S. M.: A single parameter representation of hygroscopic growth and cloud condensation nucleus activity, Atmospheric Chemistry and Physics, 7, 1961-1971, 2007.

Prather, K. A., Bertram, T. H., Grassian, V. H., Deane, G. B., Stokes, M. D., DeMott, P. J., Aluwihare, L. I., Palenik, B. P., Azam, F., Seinfeld, J. H., Moffet, R. C., Molina, M. J., Cappa, C. D., Geiger, F. M., Roberts, G. C., Russell, L. M., Ault, A. P., Baltrusaitis, J., Collins, D. B., Corrigan, C. E., Cuadra-Rodriguez, L. A., Ebben, C. J., Forestieri, S. D., Guasco, T. L., Hersey, S. P., Kim, M. J., Lambert, W. F., Modini, R. L., Mui, W., Pedler, B. E., Ruppel, M. J., Ryder, O. S., Schoepp, N. G., Sullivan, R. C., and Zhao, D.: Bringing the ocean into the laboratory to probe the chemical complexity of sea spray aerosol, Proceedings of the National Academy of Sciences, 201300262, 10.1073/pnas.1300262110, 2013.

Pratt, K. A., Hatch, L. E., and Prather, K. A.: Seasonal Volatility Dependence of Ambient Particle Phase Amines, Environmental Science & Technology, 43, 5276-5281, 10.1021/es803189n, 2009.

Pratt, K. A., and Prather, K. A.: Real-Time, Single-Particle Volatility, Size, and Chemical Composition Measurements of Aged Urban Aerosols, Environmental Science & Technology, 43, 8276-8282, 10.1021/es902002t, 2009.

Qin, X. Y., Pratt, K. A., Shields, L. G., Toner, S. M., and Prather, K. A.: Seasonal comparisons of single-particle chemical mixing state in Riverside, CA, Atmospheric Environment, 59, 587-596, 10.1016/j.atmosenv.2012.05.032, 2012.

Qiu, C., and Zhang, R. Y.: Multiphase chemistry of atmospheric amines, Physical Chemistry Chemical Physics, 15, 5738-5752, 10.1039/c3cp43446j, 2013.

Qu, W. J., Wang, J., Zhang, X. Y., Wang, D., and Sheng, L. F.: Influence of relative humidity on aerosol composition: Impacts on light extinction and visibility impairment at two sites in coastal area of China, Atmospheric Research, 153, 500-511, 10.1016/j.atmosres.2014.10.009, 2015.

Randles, C. A., Russell, L. M., and Ramaswamy, V.: Hygroscopic and optical properties of organic sea salt aerosol and consequences for climate forcing, Geophysical Research Letters, 31, 10.1029/2004gl020628, 2004.

Rehbein, P. J. G., Jeong, C.-H., McGuire, M. L., and Evans, G. J.: Strategies to Enhance the Interpretation of Single-Particle Ambient Aerosol Data, Aerosol Science and Technology, 46, 584-595, 10.1080/02786826.2011.650334, 2012.

Rissler, J., Vestin, A., Swietlicki, E., Fisch, G., Zhou, J., Artaxo, P., and Andreae, M. O.: Size distribution and hygroscopic properties of aerosol particles from dry-season biomass burning in Amazonia, Atmospheric Chemistry and Physics, 6, 471-491, 2006.

Shi, Y., Ge, M., and Wang, W.: Hygroscopicity of internally mixed aerosol particles containing benzoic acid and inorganic salts, Atmospheric Environment, 60, 9-17, 2012.

Silva, P. J., Liu, D. Y., Noble, C. A., and Prather, K. A.: Size and chemical characterization of individual particles resulting from biomass burning of local Southern California species, Environmental Science & Technology, 33, 3068-3076, 10.1021/es980544p, 1999.

Silva, P. J.: Source profiling and apportionment of airborne particles: A new approach using aerosol time-of-flight mass spectrometry, Ph.D., University of California, Riverside, United States -- California, 428-428 p. pp., 2000.

Sjogren, S., Gysel, M., Weingartner, E., Alfarra, M. R., Duplissy, J., Cozic, J., Crosier, J., Coe, H., and Baltensperger, U.: Hygroscopicity of the submicrometer aerosol at the high-alpine site Jungfraujoch, 3580 m a.s.l., Switzerland, Atmospheric Chemistry and Physics, 8, 5715-5729, 2008.

Song, X. H., Hopke, P. K., Fergenson, D. P., and Prather, K. A.: Classification of single particles analyzed by ATOFMS using an artificial neural network, ART-2A, Analytical Chemistry, 71, 860-865, 10.1021/ac9809682, 1999.

Spencer, M. T., Shields, L. G., Sodeman, D. A., Toner, S. M., and Prather, K. A.: Comparison of oil and fuel particle chemical signatures with particle emissions from heavy and light duty vehicles, Atmospheric Environment, 40, 5224-5235, 10.1016/j.atmosenv.2006.04.011, 2006.

Su, Y. X., Sipin, M. F., Furutani, H., and Prather, K. A.: Development and characterization of an aerosol time-of-flight mass spectrometer with increased detection efficiency, Analytical Chemistry, 76, 712-719, 10.1021/ac034797z, 2004.

Sullivan, R. C., Guazzotti, S. A., Sodeman, D. A., and Prather, K. A.: Direct observations of the atmospheric processing of Asian mineral dust, Atmospheric Chemistry and Physics, 7, 1213-1236, 2007.

Swietlicki, E., Hansson, H. C., Hameri, K., Svenningsson, B., Massling, A., McFiggans, G., McMurry, P. H., Petaja, T., Tunved, P., Gysel, M., Topping, D., Weingartner, E., Baltensperger, U., Rissler, J., Wiedensohler, A., and Kulmala, M.: Hygroscopic properties of submicrometer atmospheric aerosol particles measured with H-TDMA instruments in various environments - a review, Tellus Series B-Chemical and Physical Meteorology, 60, 432-469, 10.1111/j.1600-0889.2008.00350.x, 2008.

Toner, S. M., Shields, L. G., Sodeman, D. A., and Prather, K. A.: Using mass spectral source

signatures to apportion exhaust particles from gasoline and diesel powered vehicles in a freeway study using UF-ATOFMS, Atmospheric Environment, 42, 568-581, 10.1016/j.atmosenv.2007.08.005, 2008.

Varutbangkul, V., Brechtel, F. J., Bahreini, R., Ng, N. L., Keywood, M. D., Kroll, J. H., Flagan, R. C., Seinfeld, J. H., Lee, A., and Goldstein, A. H.: Hygroscopicity of secondary organic aerosols formed by oxidation of cycloalkenes, monoterpenes, sesquiterpenes, and related compounds, Atmospheric Chemistry and Physics, 6, 2367-2388, 2006.

Wang, X. N., Ye, X. N., Chen, H., Chen, J. M., Yang, X., and Gross, D. S.: Online hygroscopicity and chemical measurement of urban aerosol in Shanghai, China, Atmospheric Environment, 95, 318-326, 10.1016/j.atmosenv.2014.06.051, 2014.

Weingartner, E., Burtscher, H., and Baltensperger, U.: Hygroscopic properties of carbon and diesel soot particles, Atmospheric Environment, 31, 2311-2327, 1997.

Ye, X., Tang, C., Yin, Z., Chen, J., Ma, Z., Kong, L., Yang, X., Gao, W., and Geng, F.: Hygroscopic growth of urban aerosol particles during the 2009 Mirage-Shanghai Campaign, Atmospheric Environment, 64, 263-269, 2013.

Ye, X. N., Chen, T. Y., Hu, D. W., Yang, X., Chen, J. M., Zhang, R. Y., Khakuziv, A. F., and Wang, L.: A Multifunctional HTDMA System with a Robust Temperature Control, Advances in Atmospheric Sciences, 26, 1235-1240, 10.1007/s00376-009-8134-3, 2009.

Ye, X. N., Ma, Z., Hu, D. W., Yang, X., and Chen, J. M.: Size-resolved hygroscopicity of submicrometer urban aerosols in Shanghai during wintertime, Atmospheric Research, 99, 353-364, 10.1016/j.atmosres.2010.11.008, 2011.

Zauscher, M. D., Wang, Y., Moore, M. J. K., Gaston, C. J., and Prather, K. A.: Air Quality Impact and Physicochemical Aging of Biomass Burning Aerosols during the 2007 San Diego Wildfires, Environmental Science & Technology, 47, 7633-7643, 10.1021/es4004137, 2013.

Zelenyuk, A., Imre, D., Han, J. H., and Oatis, S.: Simultaneous measurements of individual ambient particle size, composition, effective density, and hygroscopicity, Analytical Chemistry, 80, 1401-1407, 10.1021/ac701723v, 2008.

Zhang, G., Bi, X., Chan, L. Y., Li, L., Wang, X., Feng, J., Sheng, G., Fu, J., Li, M., and Zhou, Z.: Enhanced trimethylamine-containing particles during fog events detected by single particle aerosol mass spectrometry in urban Guangzhou, China, Atmospheric Environment, 55, 121-126, 10.1016/j.atmosenv.2012.03.038, 2012.

Zhang, Q., Jimenez, J. L., Canagaratna, M. R., Allan, J. D., Coe, H., Ulbrich, I., Alfarra, M. R., Takami, A., Middlebrook, A. M., Sun, Y. L., Dzepina, K., Dunlea, E., Docherty, K., DeCarlo, P. F., Salcedo, D., Onasch, T., Jayne, J. T., Miyoshi, T., Shimono, A., Hatakeyama, S., Takegawa, N., Kondo, Y., Schneider, J., Drewnick, F., Borrmann, S., Weimer, S., Demerjian, K., Williams, P., Bower, K., Bahreini, R., Cottrell, L., Griffin, R. J., Rautiainen, J., Sun, J. Y., Zhang, Y. M., and Worsnop, D. R.: Ubiquity and dominance of oxygenated species in organic aerosols in anthropogenically-influenced Northern Hemisphere midlatitudes, Geophysical Research Letters, 34, L13801, 10.1029/2007gl029979, 2007.

876   ***ACKNOWLEDGMENT***

877   This work was supported by the National Natural Science Foundation of China (Nos. 91544224,

878   21906024, 41775150, 41827804), Shanghai Natural Science Foundation (No. 19ZR1404000)

879   and the Program for Guangdong Introducing Innovative and Entrepreneurial Teams

880   (2017ZT07Z479). We acknowledge the Shanghai Environmental Monitoring Center for

881   providing ambient air quality data.

882

 TABLES

884 Table 1. Statistics of the DRH, GF, sampling duration and the number of chemically analyzed

885 particles by ATOFMS (D_{dry} = 250 nm, RH = 85%).

D_{RH} (nm)	225	250	275	300	325	350	375	400	425
Growth Factor	0.9	1.0	1.1	1.2	1.3	1.4	1.5	1.6	1.7
Duration (hours)	42	67	11	20	8	11	34	20	11
Number of particle spectra	742	1665	709	1401	2330	4469	6399	723	262

886

887 Table 2. Statistics on particle number contributions of ATOFMS particle types to different GF

888 modes. The statistics are the average contributions and variation ranges (in brackets) based on

889 temporal data in daily resolution.

Contribution (%)	NH (GF <1.1)	LH (GF 1.1-1.3)	MH (GF 1.3-1.5)	SS (GF >1.5)
Fresh EC	14 (7-17)	2 (1-4)	0 (0-3)	0 (0-1)
Cooking	3 (0-7)	1 (0-3)	0 (0-0)	0 (0-0)
Biomass	18 (7-35)	9 (2-17)	0 (0-1)	0 (0-0)
HMOC	40 (30-68)	8 (2-15)	0 (0-1)	0 (0-0)
Ammonium/OC	11 (3-21)	32 (20-45)	2 (1-5)	0 (0-0)
Aged EC	2 (1-5)	12 (5-20)	47 (15-72)	13 (1-42)
Dust/ash	3 (1-6)	13 (9-22)	27 (13-53)	26 (4-44)
Amine-rich	3 (1-5)	12 (2-41)	13 (4-39)	11 (1-44)
Sea salt	0 (0-1)	0 (0-1)	1 (0-4)	40 (7-78)

890

891 ***FIGURES***
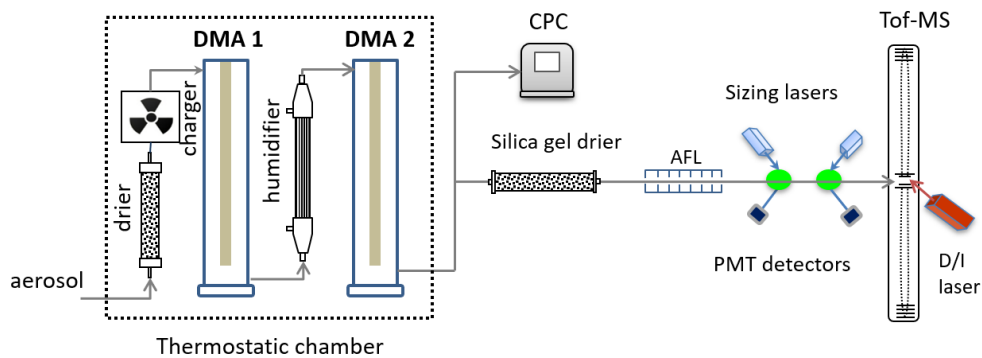
892

893 Figure 1. The schematic of HTDMA-ATOFMS characterization setup showing the major parts

894 of HTDMA (left), ATOFMS (right). The humidifier in HTDMA was maintained at 85% RH.

895
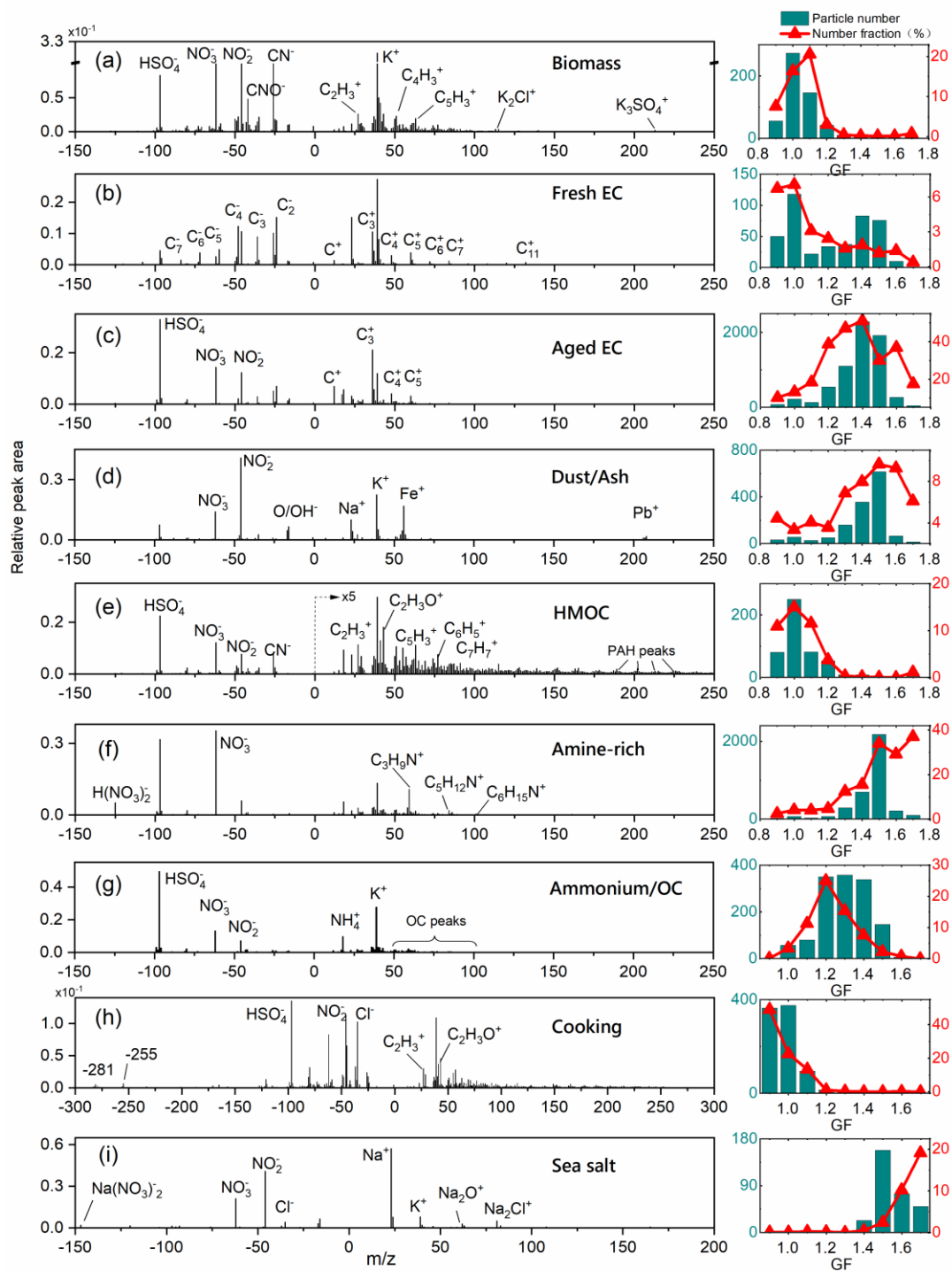
Figure 2. (Left panel) Averaged particle mass spectra of the major particle types detected in
HTDMA-ATOFMS characterization. Peaks of significance were labelled. Right panels show
the particle numbers of each type (left-axis) and their relative number fractions in total particles
(right-axis) as a function of GF.
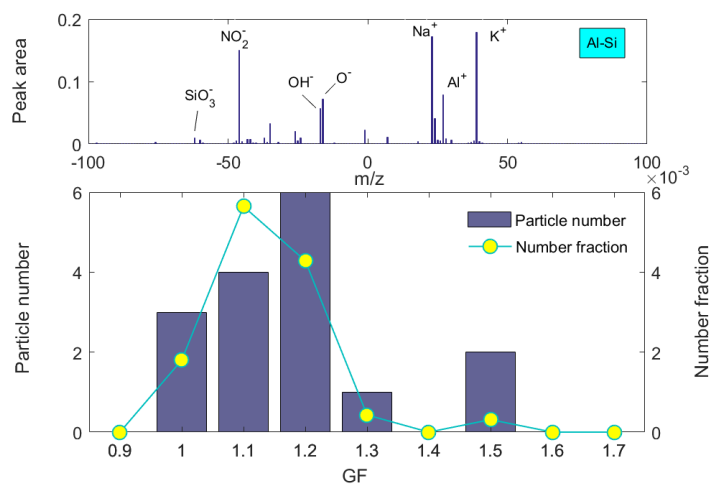
900

901   Figure 3. Average mass spectra and hygroscopicity distribution of Al-Si particles.

902
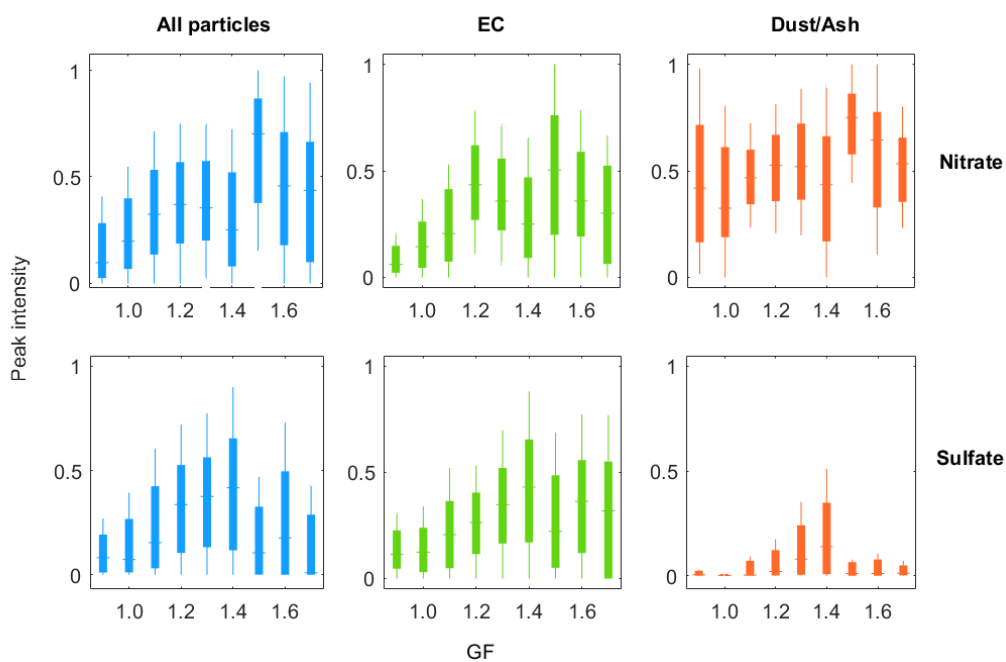
903

904   Figure 4. Statistics of nitrate and sulfate peak intensities (minimum, 25th percentile, median,

905   75th percentile, maximum) with GF in HTDMA-ATOFMS experiment. The intensity statistics

906
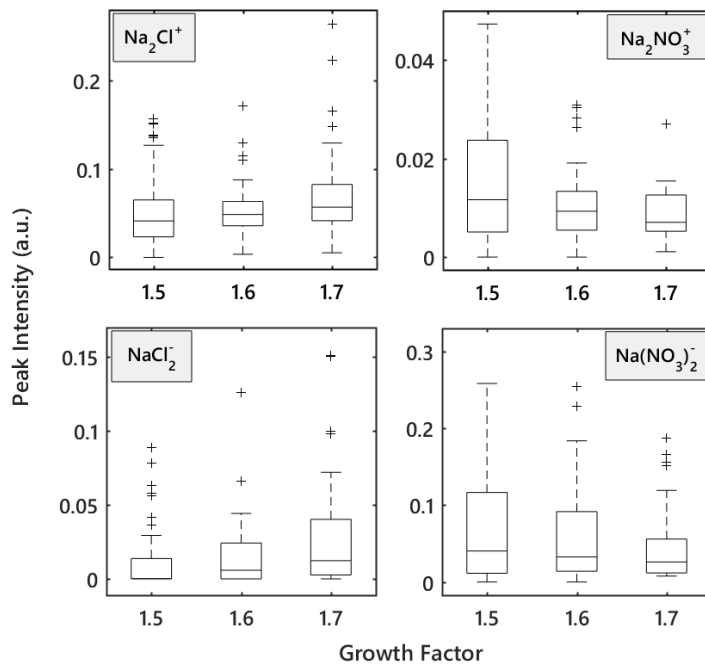
Figure 5. Statistics of peak intensities in sea salt particle mass spectra in GF 1.5-1.7 range. The statistics include minimum, 25th percentile, median, 75th percentile, maximum and outliers for each GF bin.

910

911
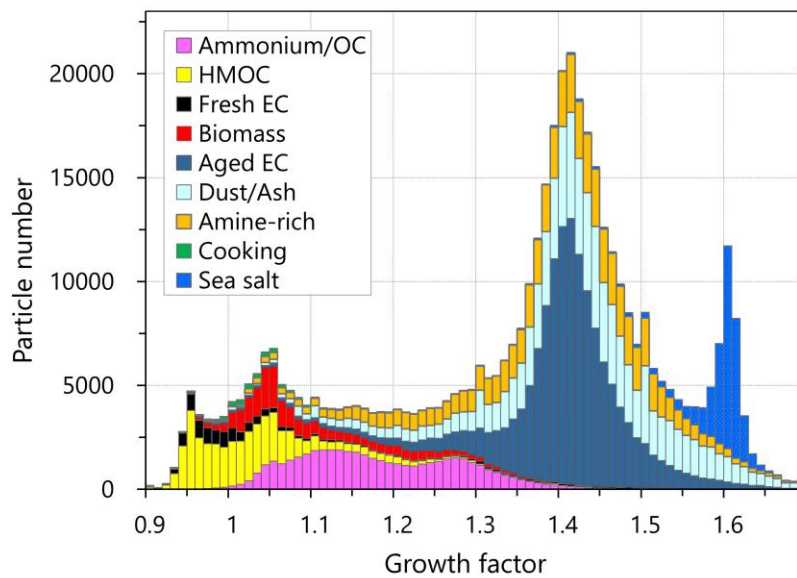
Figure 6. Particle number distribution of different particle types as a function of estimated GF during Sep-12 to Sep-28, 2012.
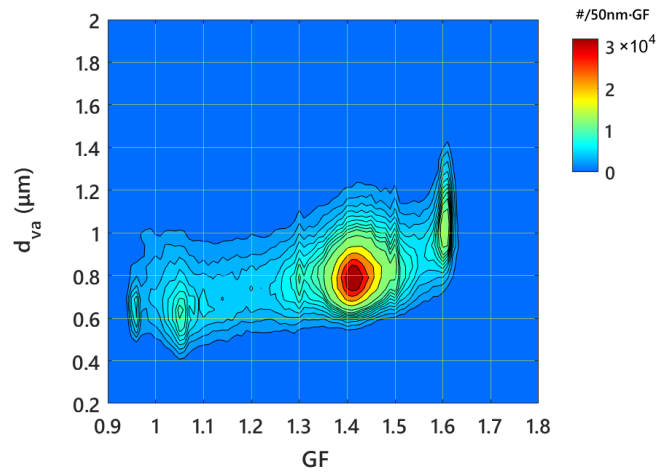
914

915 Figure 7. The distribution of ATOFMS particles as a bivariate function of estimated GF and

916 aerodynamic diameter.

917
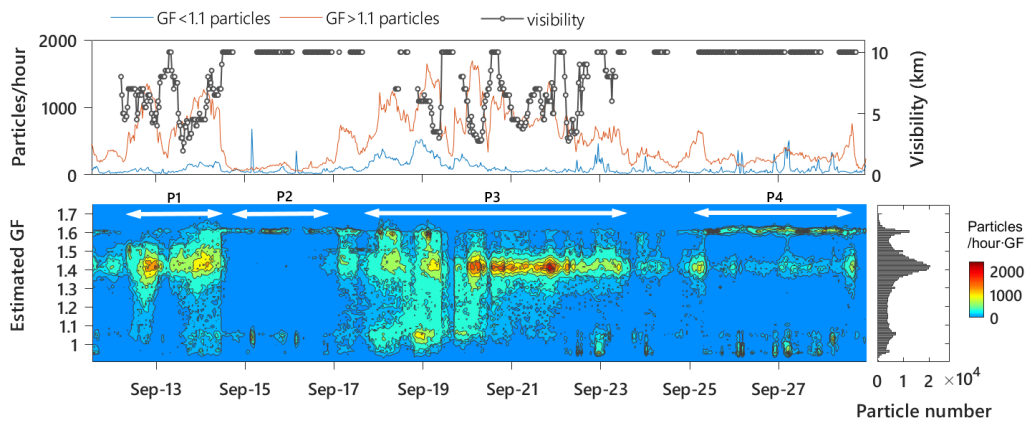
918

919 Figure 8. Temporal variations of atmospheric visibility and number concentrations of nearly-

920 hydrophobic (estimated GF < 1.1) and hygroscopic (GF >1.1) particles (Upper). The lower

921 panel show the temporal variation of estimated GF from Sep-12 to Sep-28, 2012. In the lower-

922 right panel is the particle number distribution with GF during the period.

923

924
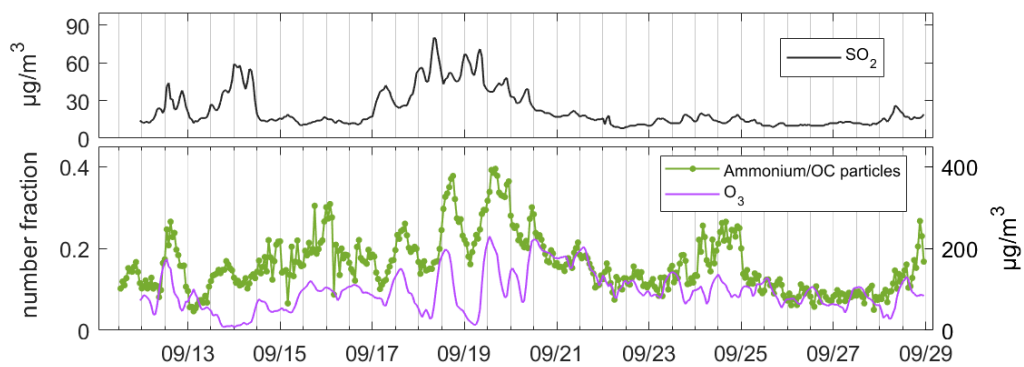
Figure 9. Temporal traces of Ammonium/OC relative number concentrations, ambient O_3 and

SO$_2$ concentrations during Sep-12 to Sep-28, 2012

927

928
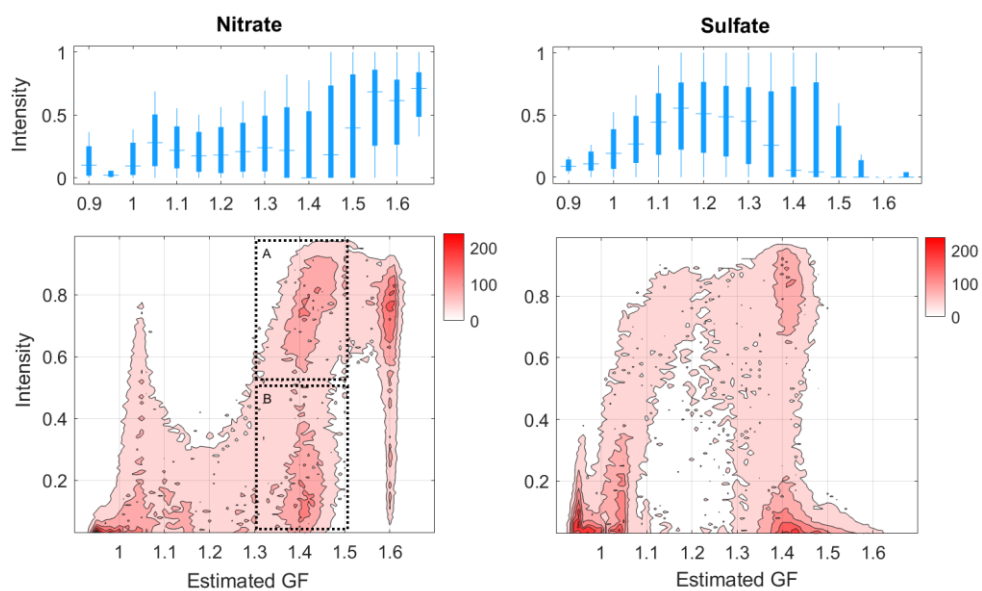
Figure 10. Statistics (minimum, 25th percentile, median, 75th percentile, maximum) on the nitrate

and sulfate peak intensities of ambient particles at different GFs (upper). The lower panels show

particle distributions as a bivariate function of estimated GF and peak intensities of nitrate and

sulfate.
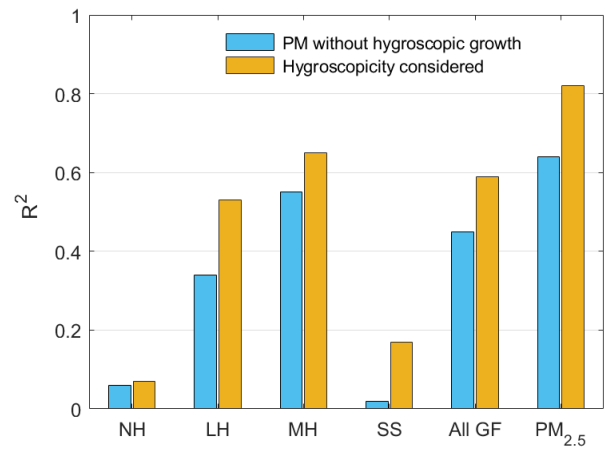
933

934   Figure 11. The R-squares between visibility and PM volume concentrations with and without

935   considering particle hygroscopicity

936